Replies to Referee 2

Before replying to Referee 2, the authors wish to thank Referee 2 to read and provide a thorough review of our manuscript, including constructive critics and suggestions.

Major concerns:

1) Applicability of 30-day runs for evaluating "average" model state, systematic biases.

In response to the concern that "30 days is a duration that does not fit neatly into one of these bins", and as suggested by the reviewer, we compare the 10-day mean calculated between 00 UTC 1 Dec. and 00 UTC 11 Dec. 2015 against the full monthly mean for most of the diagnostics discussed in our manuscript. The file "RepliesReferee2.AdditionalFigs.pdf" includes most of the same figures as those shown in our manuscript and displays 10-day mean instead of monthly-mean diagnostics. The figure captions are the same as those in our manuscript, except for adding an "r" after the figure number. In contrast to Fig. 5, the left panels of Fig. 5r show the 10-day mean LWP, IWP, and CLD instead of monthly-mean SSF1deg data.

Comparing the figures from "RepliesReferee2.AdditionalFigs.pdf" compared to their respective figures from our manuscript highlights that GFu, GFv, MSKFu, andMSKFv, display similar errors in days 1-10 when compared to their full monthly means. In particular:

- Figure 11r displays similar biases in the total precipitation rate produced with GFu, GFv, MSKFu, and MSKFv when compared to TMPA data, including the bias in the location of the ITCZ over the Tropical Pacific Ocean, as pointed out by Referee 2.
- Figures 14r and 17r display similar biases in the LWP and IWP produced with the four simulations when compared against the 10-day mean SSF data, leading to similar biases in the TOACLD, TOALW, and TOASW over the Tropical Pacific Ocean.
- Finally, the different figures "from RepliesReferee2.AdditionalFigs.pdf" display patterns in the 10-day mean diagnostics as in the monthly-mean diagnostics over the transition zone between the coarse and refined area of the mesh, as seen in the various GFv-GFu and MSKFv-MSKFu panels.

The authors hope that adding this set of figures will help Referee 2 conclude that the discussed biases are mostly independent of how the averaged model state was computed. The fact that 10-mean diagnostics show similar biases as monthly-mean diagnostics will help further understand the strong upscaling effect of the refined grid mesh on the coarse grid mesh, as proposed in Section 6.

2) Potential sensitivity of moist results to A) physics timestep and B) numerical diffusion.

A) Physics timestep: In MPAS, the physics timestep used in the Noah land surface scheme, the MYNN Planetary boundary layer and surface layer schemes, the Hong et al. gravity wave-drag scheme, and the deep and shallow convection schemes is the same as the dynamical timestep, i.e. 150s for the U runs and 30s for the V runs. For these physics schemes, we confirm the timestep reduction between the U and V runs is for "both" the dynamics and physics. The RRTMG longwave and shortwave radiation schemes are run every 15mns for the U and V runs. The recommended maximum timestep is 90s for the Thompson cloud microphysics scheme. Whereas the cloud microphysics timestep is the same as the dynamic timestep for the V runs, the microphysics timestep is set to 75s in the U runs w, and cloud microphysics is sub-cycled twice in the U runs.

B) Numerical diffusion: In MPAS, numerical diffusion follows the horizontal filtering formulation of Smagorinsky (1963), as described in Skamarock et al. (Eq. 17; 2012). In Eq. 17, l is the horizontal length scale which is defined as the minimum distance between cell centers, and weighted as a function the mesh density, and therefore as a function of the mesh resolution. In Table 1, while l is

equal to 30 km for the uniform-resolution experiments GFu and MSKFu since the mesh density is equal to 1, the minimum l value is set to 6 km in GFv and MSKFv, and weighted by a scaling factor which depends in the spatially-varying mesh density. Therefore, numerical diffusion takes into account the grid mesh resolution.

3) Time step:

As suggested, we ran a 10-day experiment using the GFu configuration, but with a 30s time step as in GFv (see Fig. 2S). We did see increased in convective precipitation between the 2 configurations in GFu which we attempted to address this point in Section 4.2. We agree that this result needs to be analyzed in more details. On the top of a better understanding on the partitioning between the LWP and IWP over the refined area of the mesh, this is another item that we are currently working on in greater details by looking at the contribution of the different closures to the observed increase in the convective parameterization.

Minor comments:

Line 148: Corrected typo.

Lines 175-176: The reason behind choosing one closure for the shallow convection scheme is the following: While first testing the implementation of the GF deep and shallow convection schemes, Dr. Grell suggested to test a few other closures for the shallow scheme. While the default option for the GF deep convection scheme is to use an ensemble of closures whereas the default option for the GF shallow convection scheme is to use the single *BLQE* closure, first proposed by Dr. Freitas. In the end, we choose to use the default options for the GF deep and shallow scheme, as first proposed and tested by Grell and Freitas (2014). We hope that this explanation will satisfy Referee 2.

Line 194: As suggested, we added an extra sentence related to the 0.7 threshold in σ. This sentence is similar to that in Fowler et al. (2016). As the use of this threshold was described in Fowler et al. (2016), the first author thought that a more detailed explanation was not required. Thank you.

Lines 201-211: Rephrased. The first author meant to say that the minimum thickness of the mixed layer is set to 50 hPa, meaning that for mixed layers to be identified as initial potential source layers for convection, they must be at least 50 hPa thick.

Line 316: Rephrased. In that sentence, the first author was trying to distinguish between the complexity of condensation and precipitation processes in cloud microphysics parameterizations such as WSM6 and THOM, and the simple conversion from condensed water to precipitation in simpler cloud models used in parameterizations of convection.

Line 412: In Fig. 5, the authors were trying to understand the difference in the IWP computed from the SSF data (Fig. 5.c) versus that provided in the SSF1deg data (Fig. 5.d). As stated lines 406-407, our method to compute the IWP is much simpler than that used by the CERES Science Team, and we do not have details on how the Science Team computed the IWP provided in the SSF1deg data.

Lines 513-515:

Line 532: Replaced “evaluated” with “compared”.

Lines 537-538: Replaced Figs 10.b,e and Figs. 11a,d with Figs. 10.b-e and Figs. 11.a-d.

Fig. 12: Done.

Lines 622-624: Not being an expert on satellite retrievals, it is difficult for the first author to define a “true” way for satellites to best observe the liquid and and rain water paths, separately. Section 1 summarizes the large discrepancies in the LWP and IWP between satellite-derived data sets and highlights differences in the LWP (IWP) derived from passive and active sensors. It is my understanding that in satellite retrievals, separating suspended from precipitating condensates is based on using threshold methods, but that methods

vary between satellite retrievals. It remains very difficult to compare satellite-retrieved versus simulated condensates. Another approach would be for MPAS to calculate radiances or radar reflectivities measured by satellites using cloud simulators, as sometimes done with climate models.

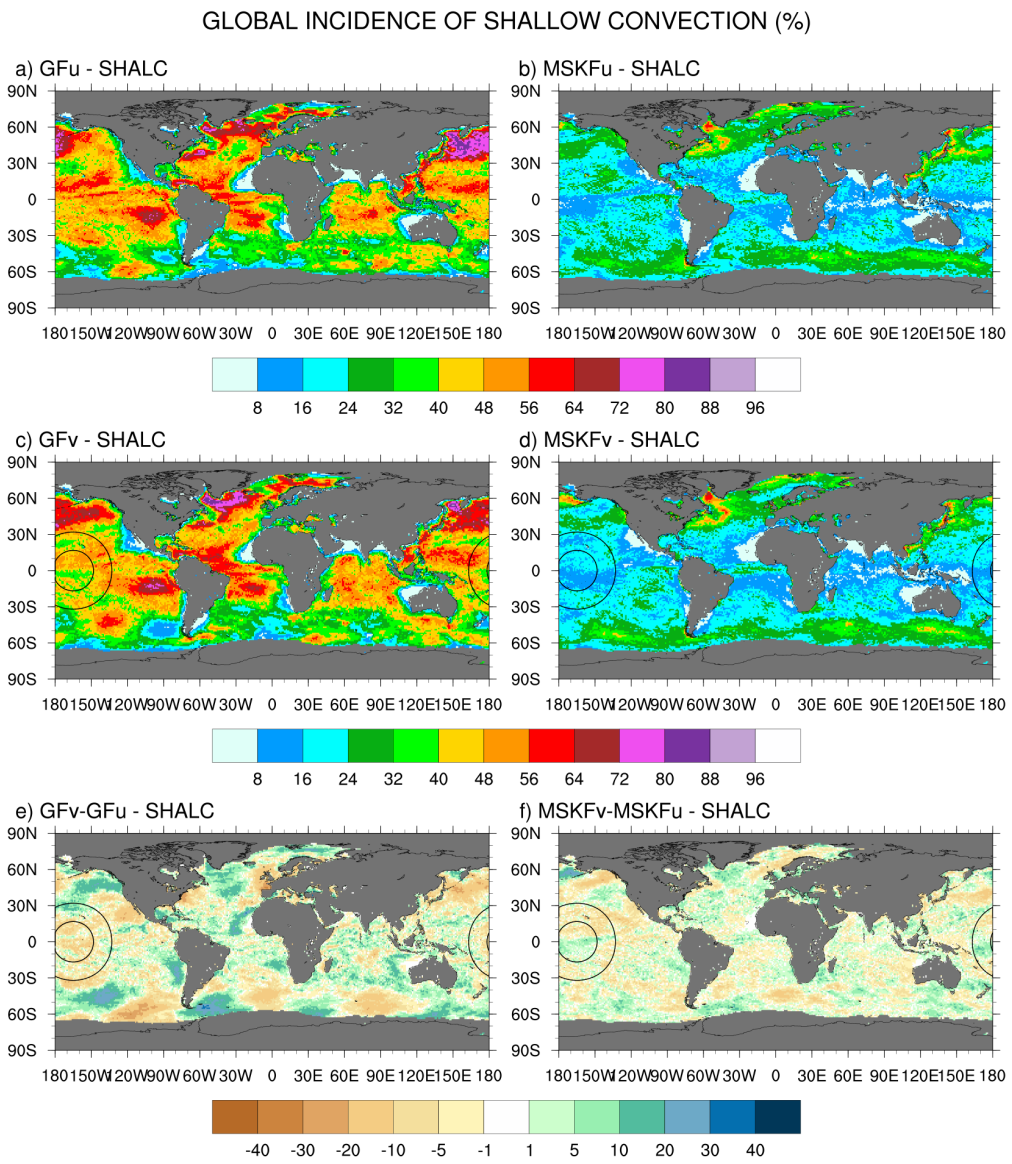

Figure 6: Global monthly-mean incidence of shallow convection (SHALC) simulated in GFu and MSKFu (top panels), and GFv and MSKFv (middle panels), and difference in the incidence of shallow convection between GFv and GFu (bottom left panel) and MSKFv and MSKFu (bottom right panel) for December 2015.

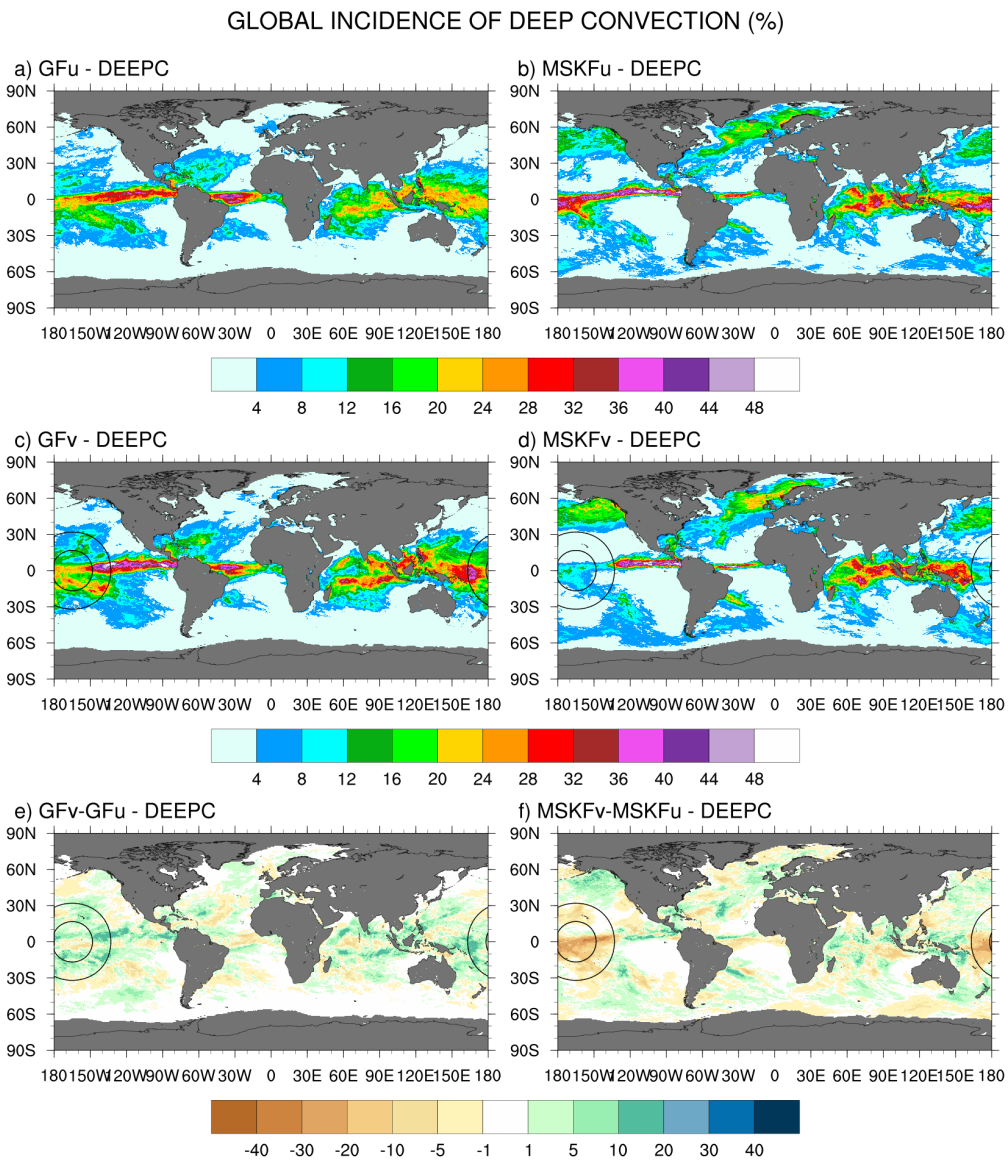

Figure 7: As Fig. 6, but for the global monthly-mean incidence of deep convection (DEEPC).

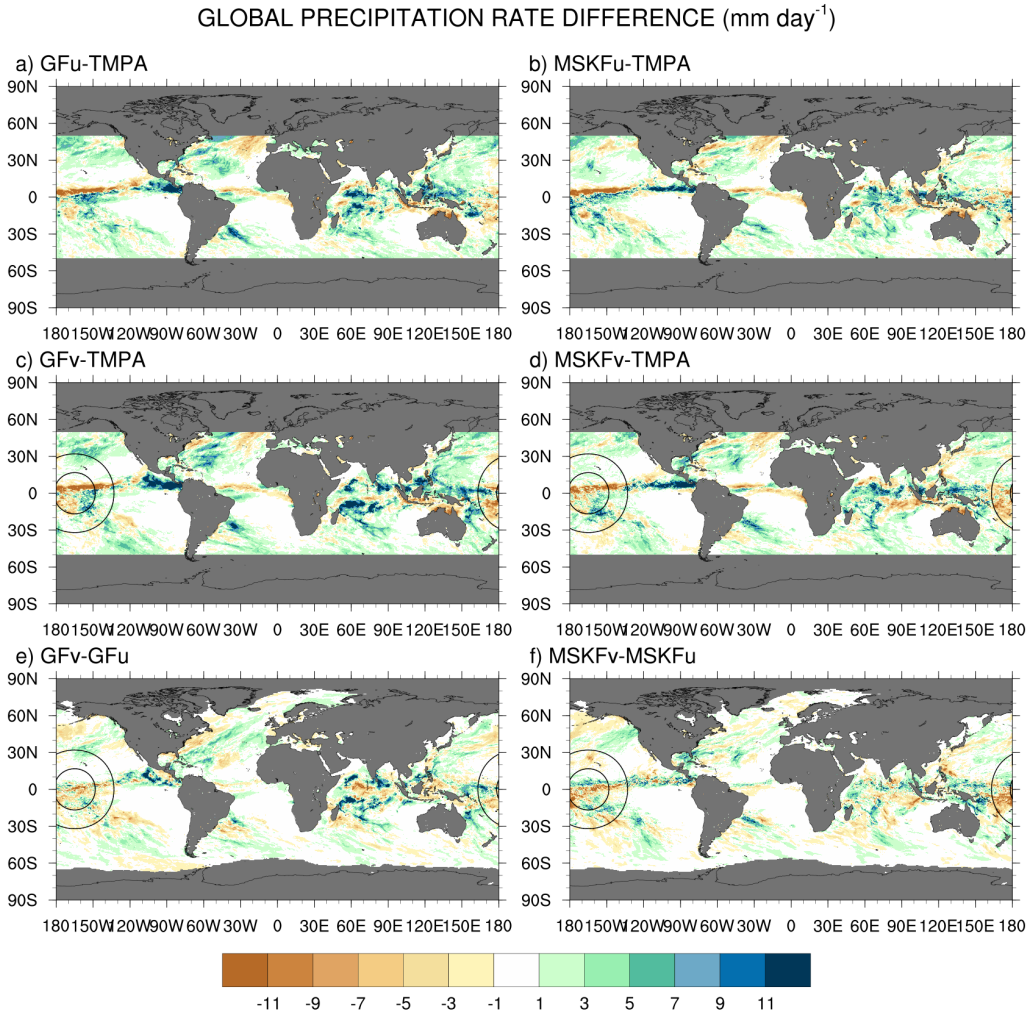

Figure 11: Global monthly-mean precipitation rate difference between GFu (MSKFu) and TMPA data (top panels), GFv (MSKFv) and TMPA data (middle panels), and between GFv (MSKFv) and GFu (MSKFu) (bottom panels) for December 2015.

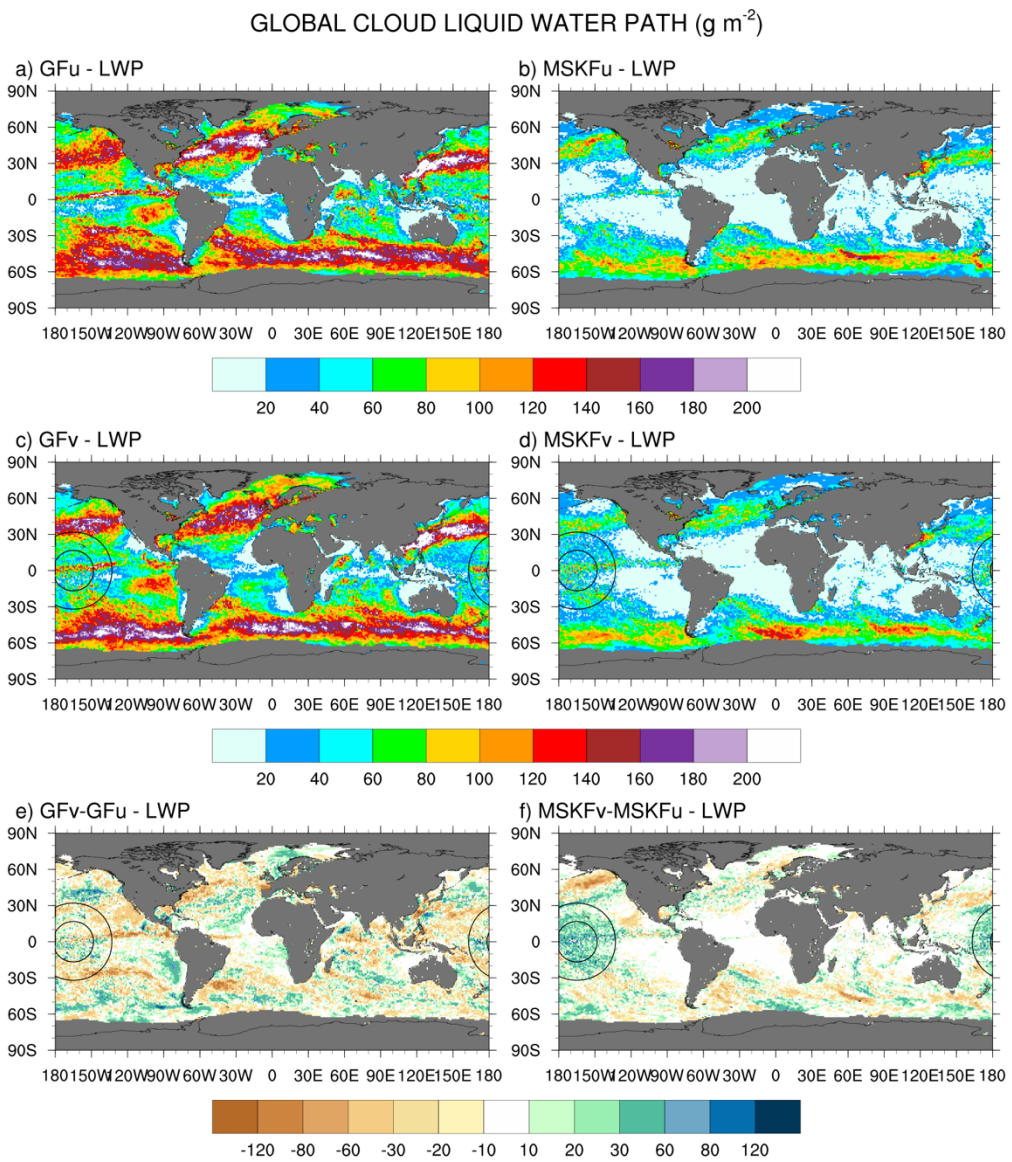

Figure 14: Global monthly-mean cloud liquid water path (LWP) simulated with GFu and MSKFu (top panels) and GFv and MSKFv (middle panels), and global monthly-mean LWP difference between GFv and GFu, and MSKFv and MSKFu (bottom panels) for December 2015.

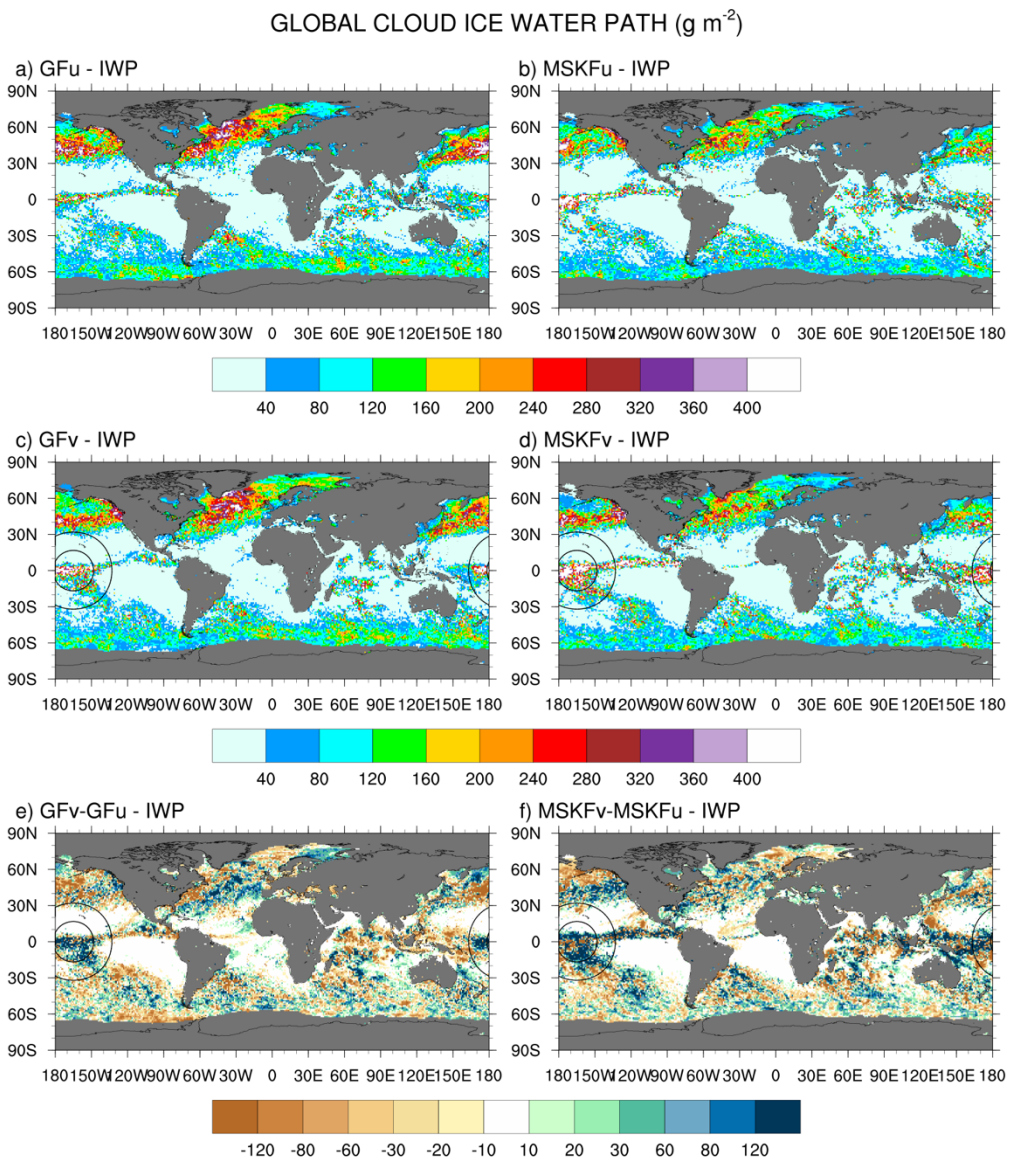

Figure 17: As Fig. 14, but for the cloud ice water path (IWP)

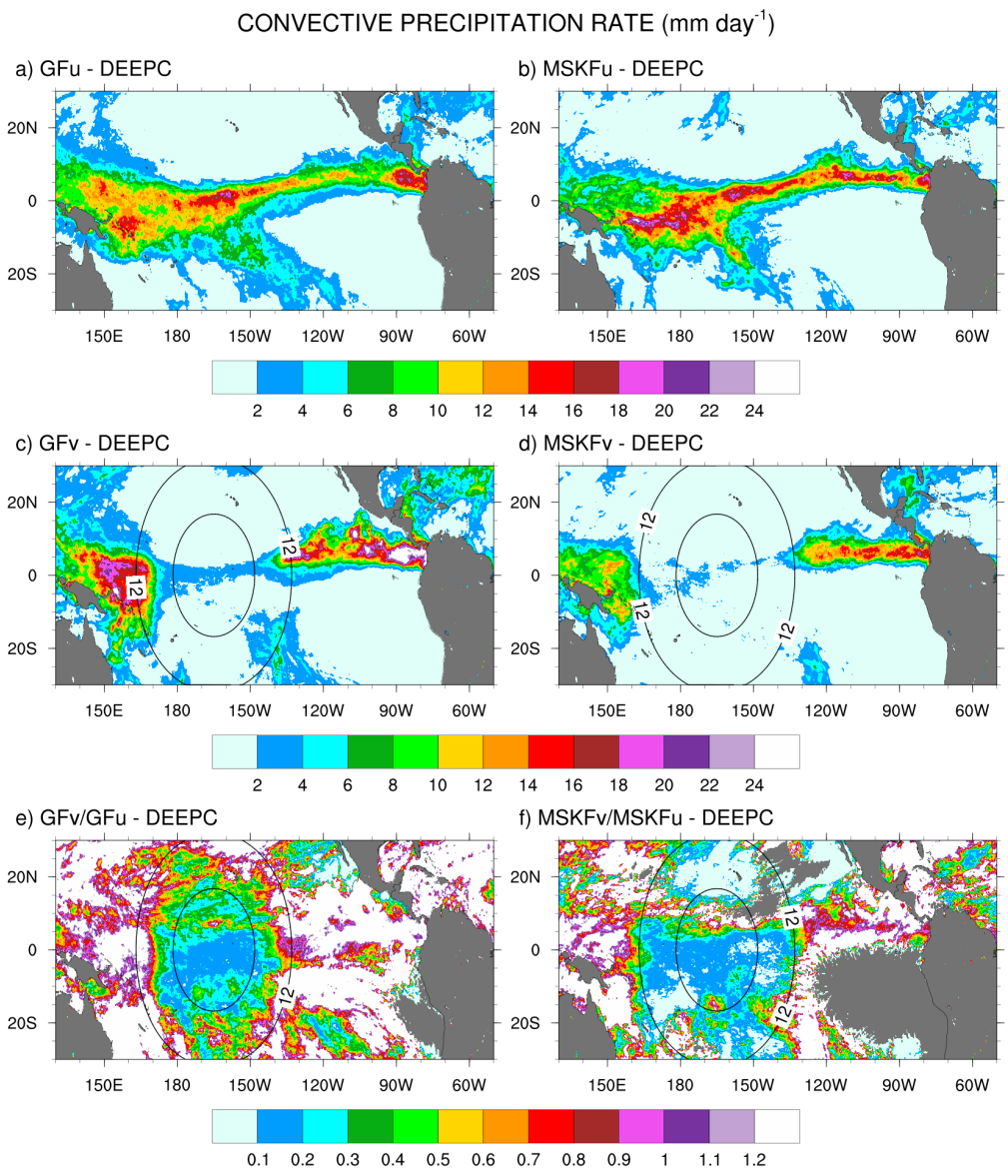

Figure A1: Monthly-mean convective (DEEPC) precipitation rate over the Tropical Pacific Ocean simulated in GFu and MSKFu (top panels) and GFv and MSKFv (bottom panels) for December 2015.

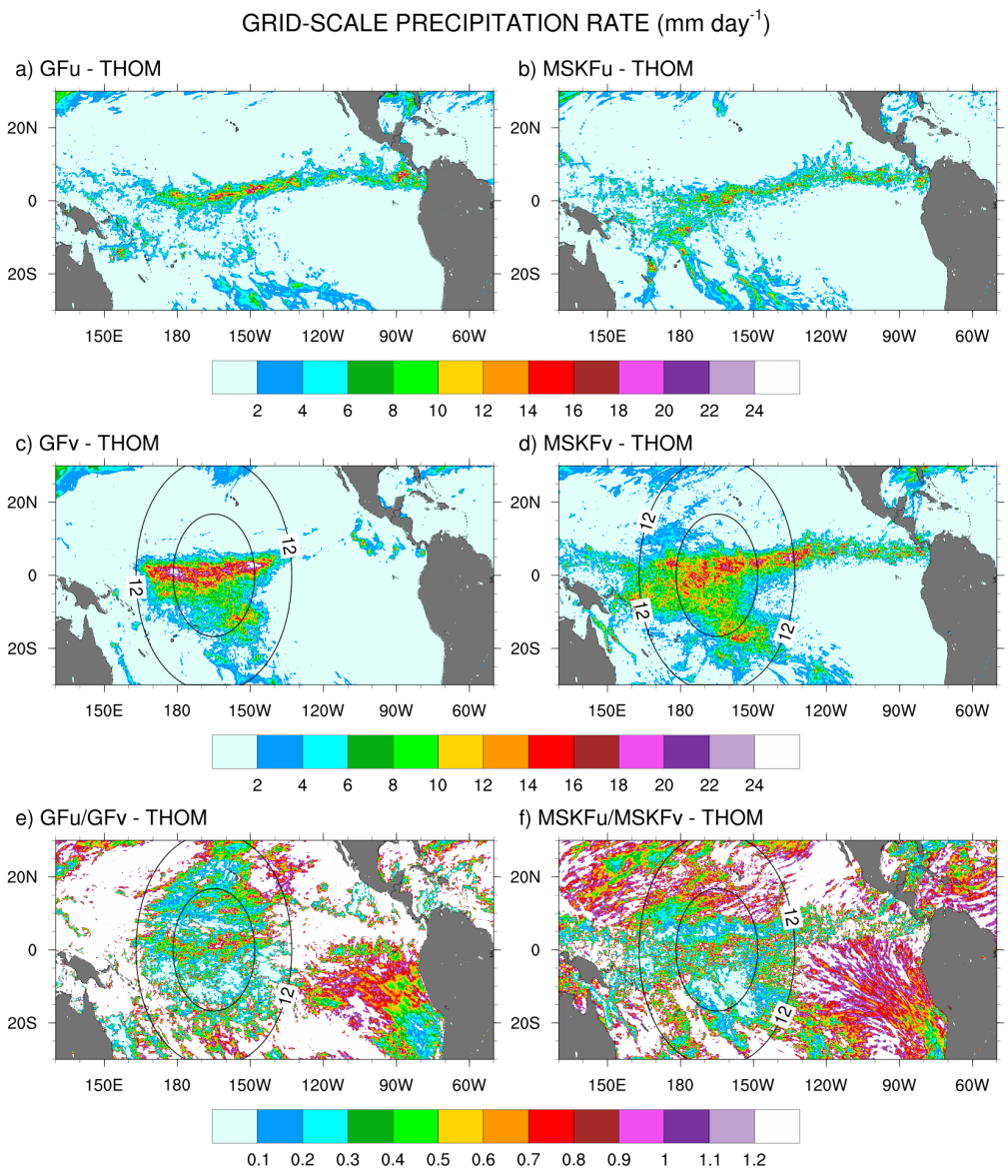

Figure A2: As Fig. A1, but for the monthly-mean grid-scale (THOM) precipitation rate.

List of Additional Figures in response to "Major concerns 1) Applicability of 30-day runs for evaluating "average" model state, systematic biases" from Referee 2.

Figure 4r: 10 day-mean cloud liquid water path (LWP, top panels), cloud ice water path (IWP, middle panels), and cloud fraction (CLD, bottom panels) over the Tropical Pacific Ocean for December 2015 from the Aqua satellite. Panels a), c), and e) are for the lower cloud layer; panels b), d), and f) are for the upper cloud layer.

Figure 5r: Cloudy area-weighted cloud liquid water path (LWP, top panels), cloudy area-weighted cloud ice water (IWP, middle panels), and cloud fraction (bottom panels) over the Tropical Pacific Ocean for December 2015. Panels a), c), and e) are monthly-mean SSF data; panels b), d), and f) are 10-day mean SSF data.

Figure 6r: 10-day mean incidence of shallow convection (SHALC) over the Tropical Pacific Ocean simulated in GFu and MSKFu (top panels) and GFv and MSKFv (middle panels), and difference in the incidence of shallow convection between GFv and GFu (bottom left panels) and MSKFv and MSKFu (bottom right panels).

Figure 7r: As Fig. 6r, but for the 10-day mean incidence of deep convection (DEEPC).

Figure 8r: 10-day mean convective (DEEPC) precipitation rate over the Tropical Pacific Ocean simulated in GFu (top panels) and GFv and MSKFv (bottom panels).

Figure 9r: As Fig. 8r, but for the 10-day mean grid-scale (THOM) precipitation rate.

Figure 10r: 10-day mean total precipitation over the Tropical Pacific Ocean from TMPA data (top panel) and simulated with GFu and MSKFu (middle panels) and GFv and MSKFv (bottom panels).

Figure 11r: 10-day mean precipitation rate difference over the Tropical Pacific Ocean between GFu (MSKFu) and TMPA data (top panels), GFv (MSKFv) and TMPA data (middle panels), and between GFv (MSKv) and GFu (MSKFu) (bottom panels).

Figure 14r: 10-day mean cloud liquid water path (LWP) over the Tropical Pacific Ocean simulated with GFu and MSKFu (top panels) and GFv and MSKFv (middle panels), and 10-day mean LWP differences between GFv and GFu, and MSKFv and MSKFu (bottom panels).

Figure 17r: As Fig. 14r, but for the cloud ice water path (IWP).

Figure S4r: 10-day mean vertically-integrated cloud fraction (TOACF) over the Tropical Pacific Ocean from a) CERES-SSF data, and difference in the TOACF between GFu (MSKFu) and CERES-SSF (middle panels) and between GFv (MSKFv) and CERES-SSF (bottom panels) for December 2015.

Figure S5r: 10-day mean TOA upward longwave radiation (TOALW) over the Tropical Pacific Ocean from a) CERES-SSF data, and difference in the TOALW between GFu (MSKFu) and CERES-SSF (middle panels) and between GFv (MSKFv) and CERES-SSF (bottom panels).

Figure S6r: As Fig. S5r, but for the TOA net shortwave radiation (TOASW).

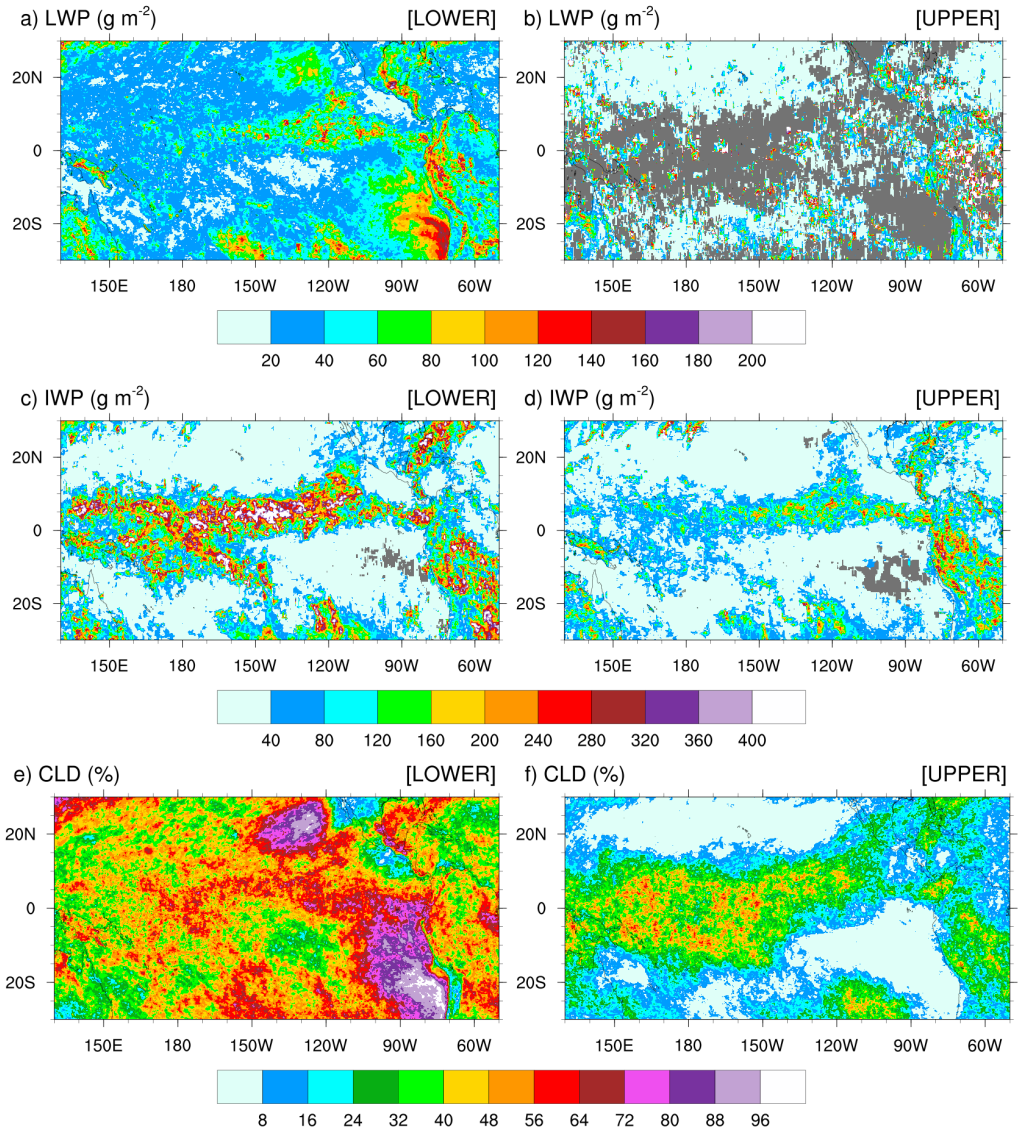

Figure 4r: 10 day-mean cloud liquid water path (LWP, top panels), cloud ice water path (IWP, middle panels), and cloud fraction (CLD, bottom panels) over the Tropical Pacific Ocean for December 2015 from the Aqua satellite. Panels a), c), and e) are for the lower cloud layer; panels b), d), and f) are for the upper cloud layer.

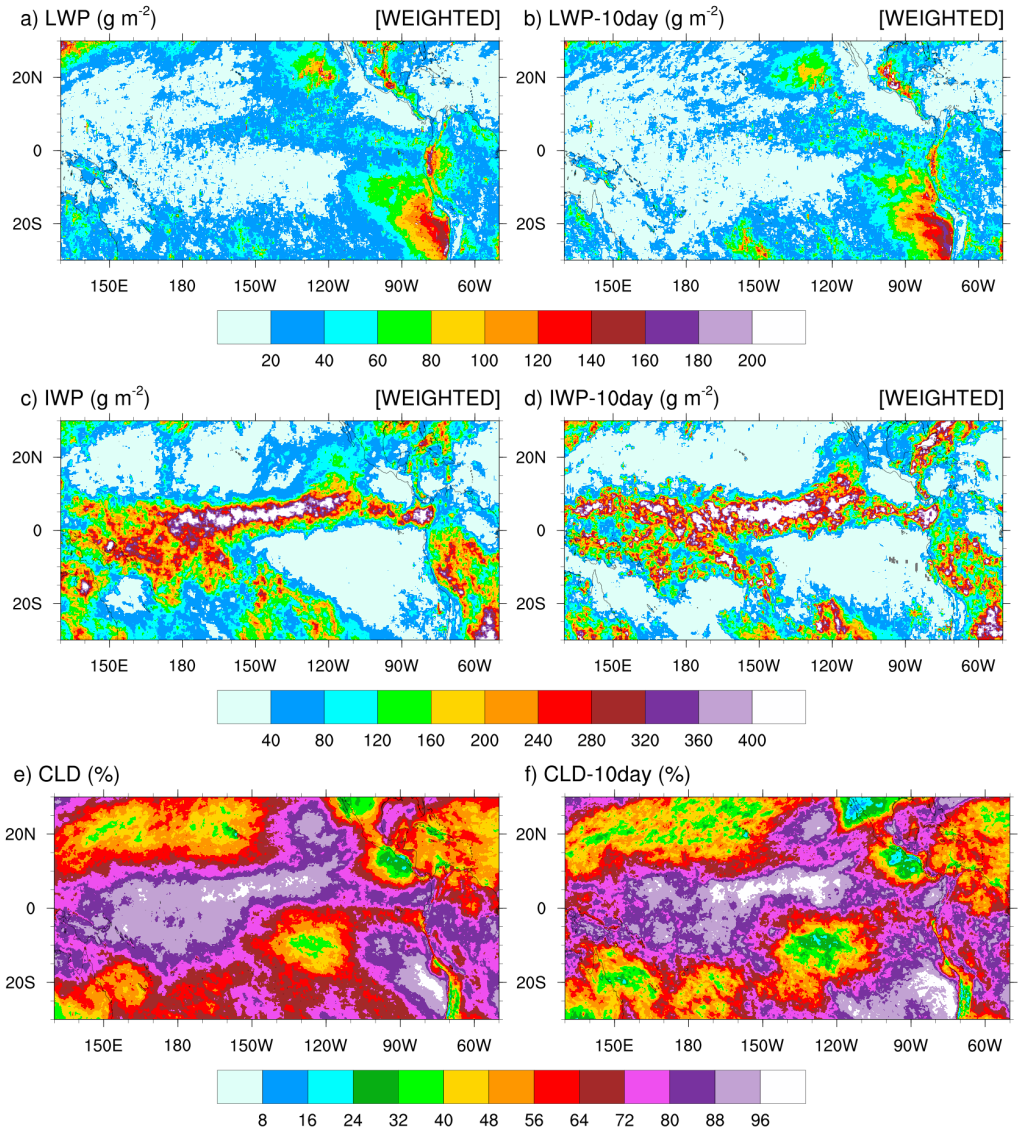

Figure 5r: Cloudy area-weighted cloud liquid water path (LWP, top panels), cloudy area-weighted cloud ice water (IWP, middle panels), and cloud fraction (bottom panels) over the Tropical Pacific Ocean for December 2015. Panels a), c), and e) are monthly-mean SSF data; panels b), d), and f) are 10-day mean SSF data.

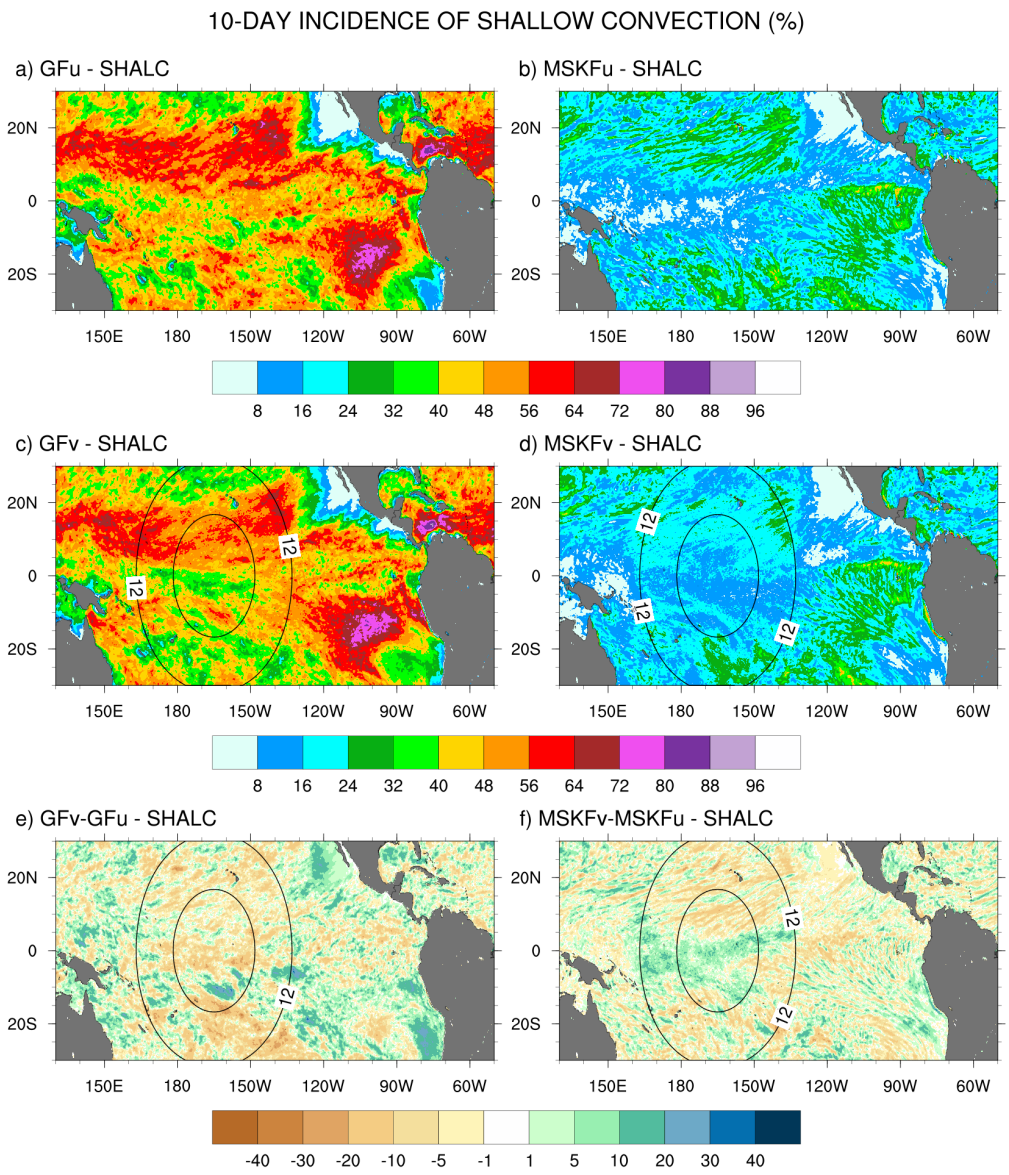

Figure 6r: 10-day mean incidence of shallow convection (SHALC) over the Tropical Pacific Ocean simulated in GFu and MSKFu (top panels) and GFv and MSKFv (middle panels), and difference in the incidence of shallow convection between GFv and GFu (bottom left panels) and MSKFv and MSKFu (bottom right panels).

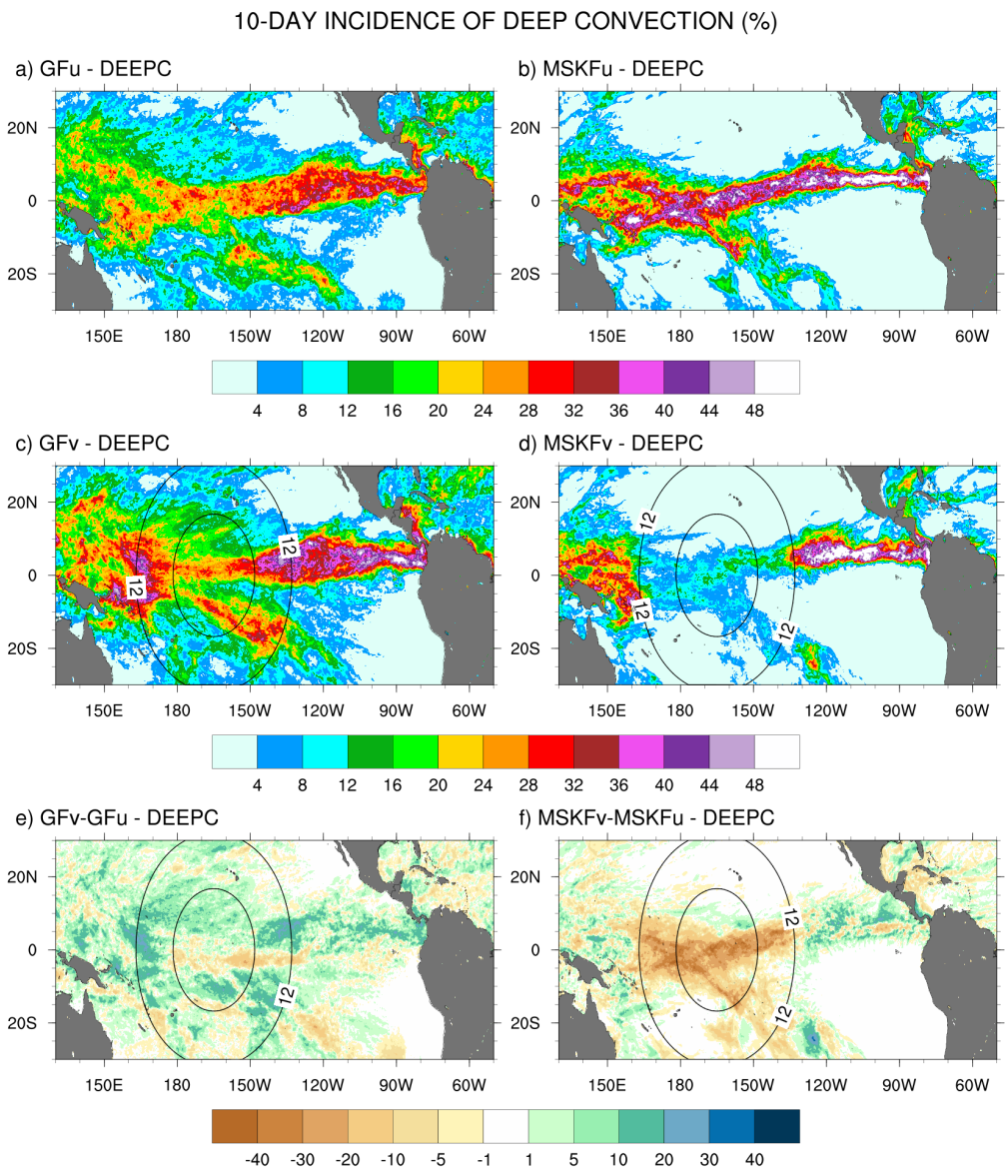

Figure 7r: As Fig. 6r, but for the 10-day mean incidence of deep convection (DEEPC).

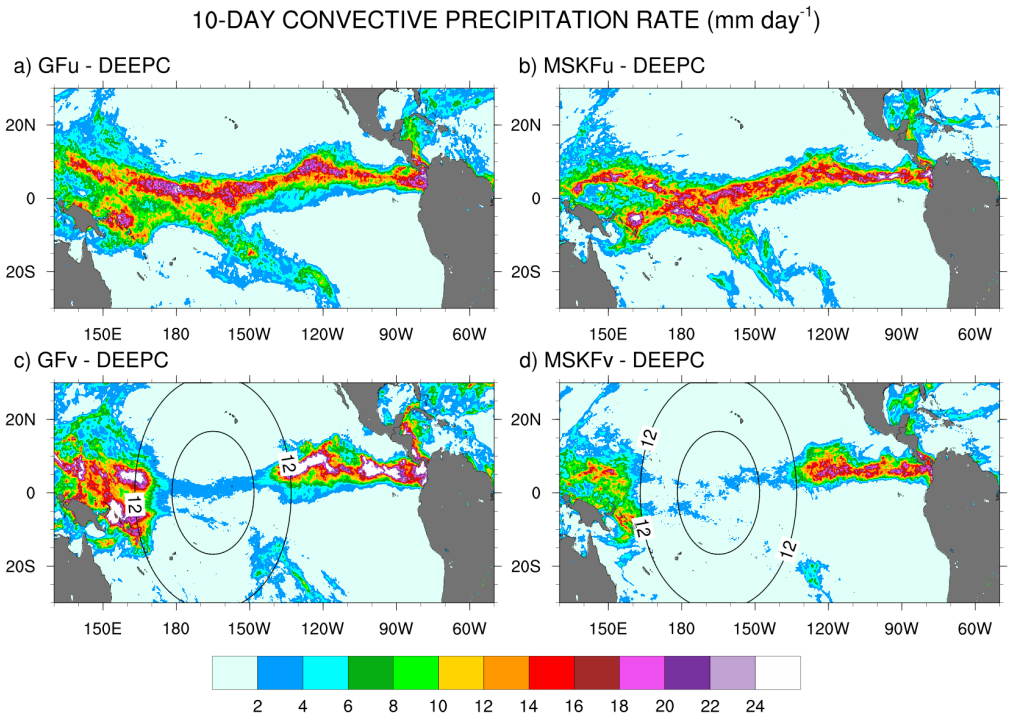

Figure 8r: 10-day mean convective (DEEPC) precipitation rate over the Tropical Pacific Ocean simulated in GFu (top panels) and GFv and MSKFv (bottom panels).

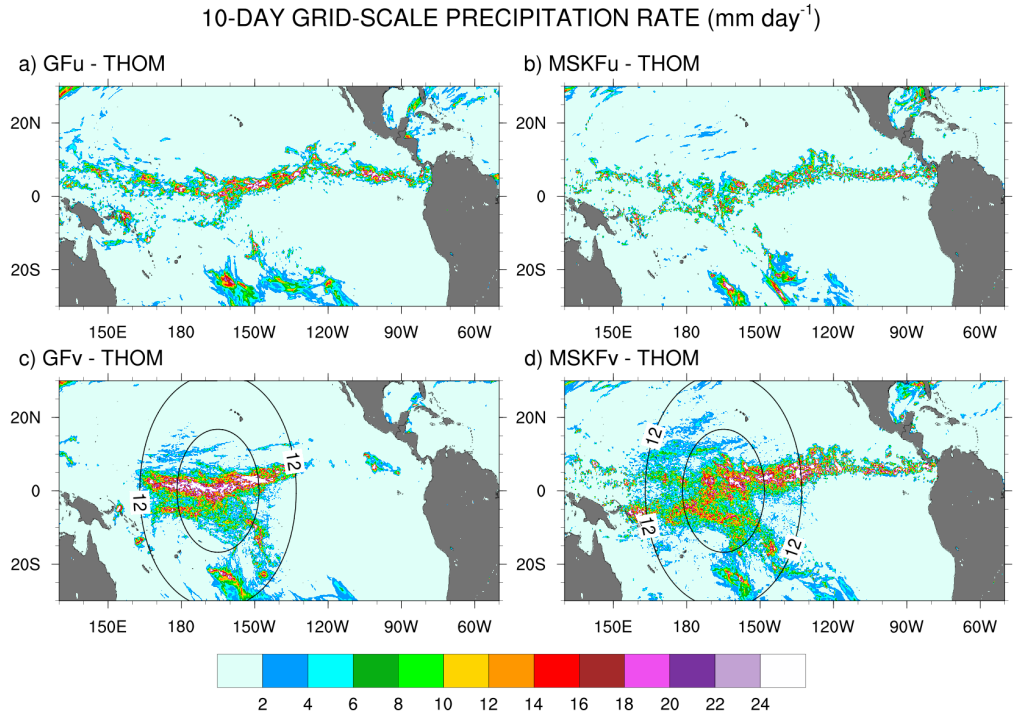

Figure 9r: As Fig. 8r, but for the 10-day mean grid-scale (THOM) precipitation rate.

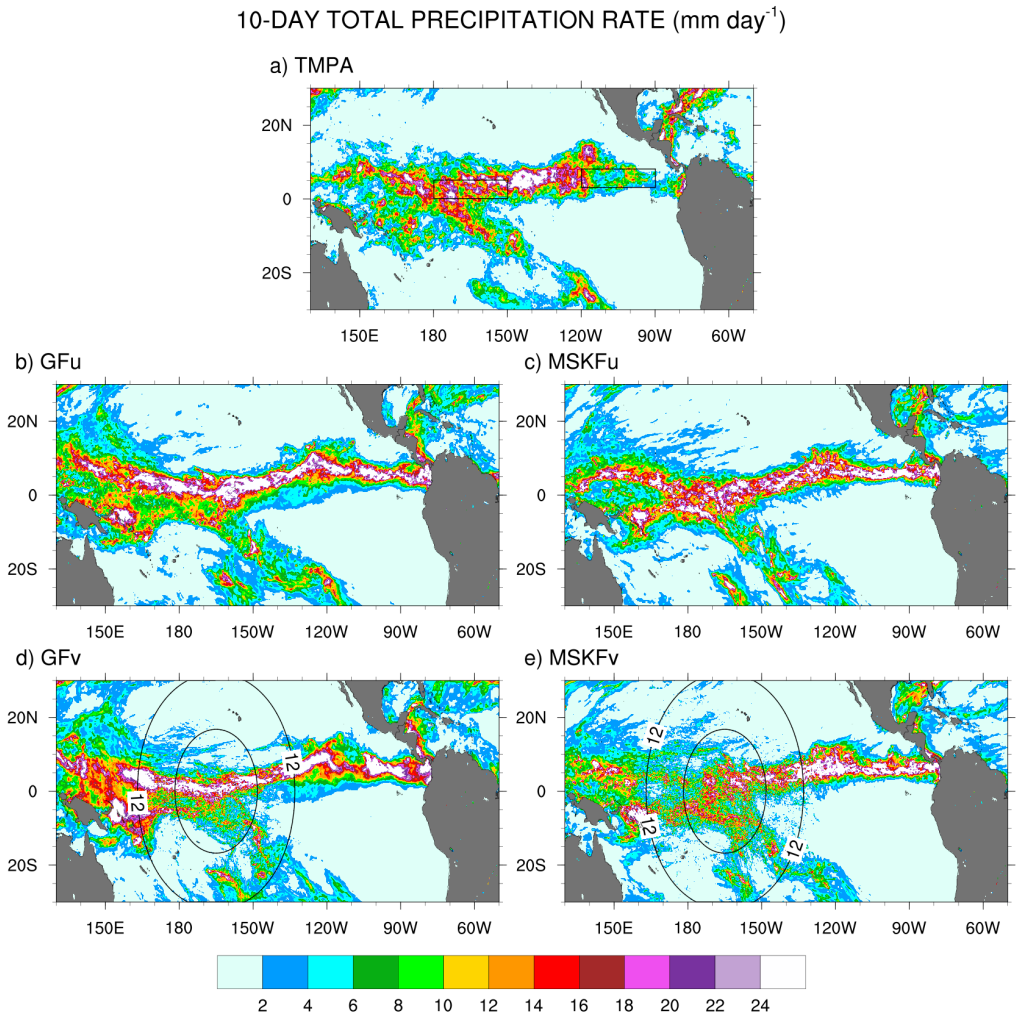

Figure 10r: 10-day mean total precipitation over the Tropical Pacific Ocean from TMPA data (top panel) and simulated with GFu and MSKFu (middle panels) and GFv and MSKFv (bottom panels).

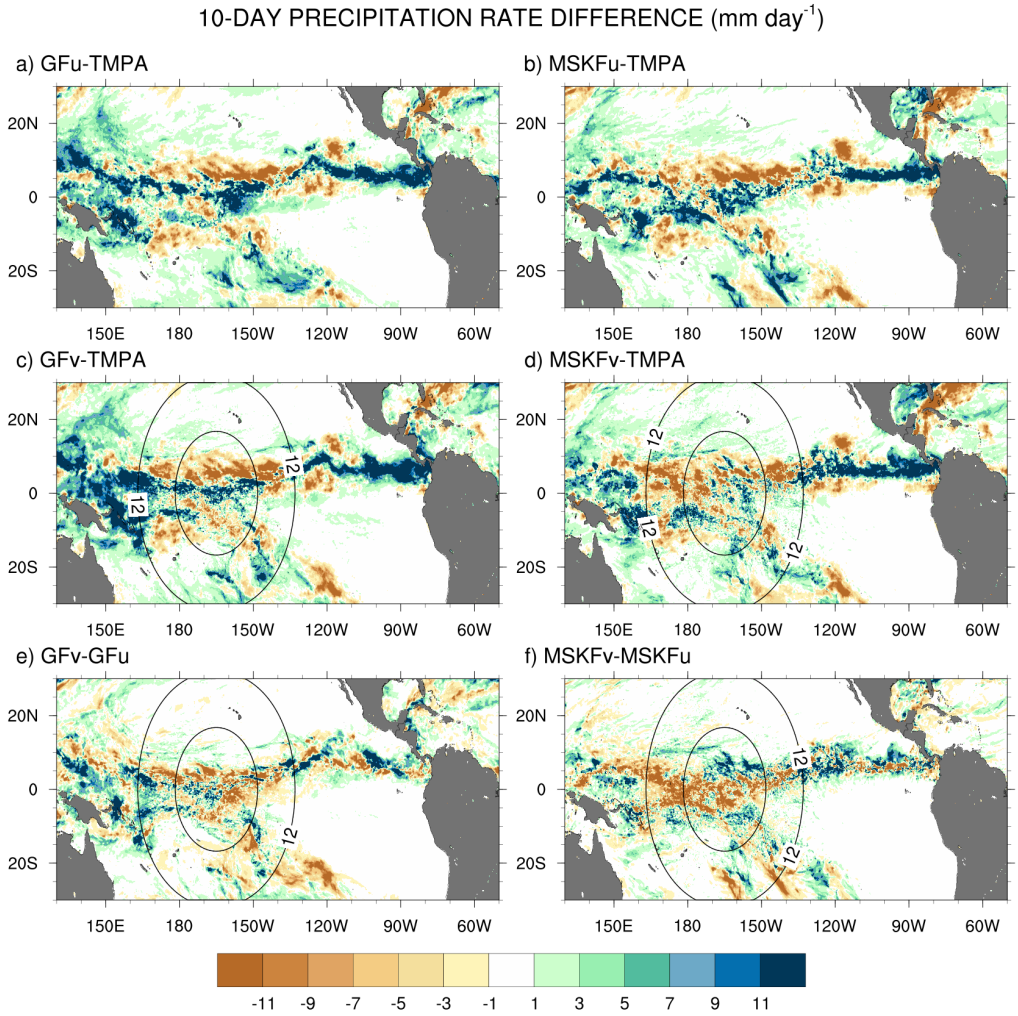

Figure 11r: 10-day mean precipitation rate difference over the Tropical Pacific Ocean between GFu (MSKFu) and TMPA data (top panels), GFv (MSKFv) and TMPA data (middle panels), and between GFv (MSKv) and GFu (MSKFu) (bottom panels).

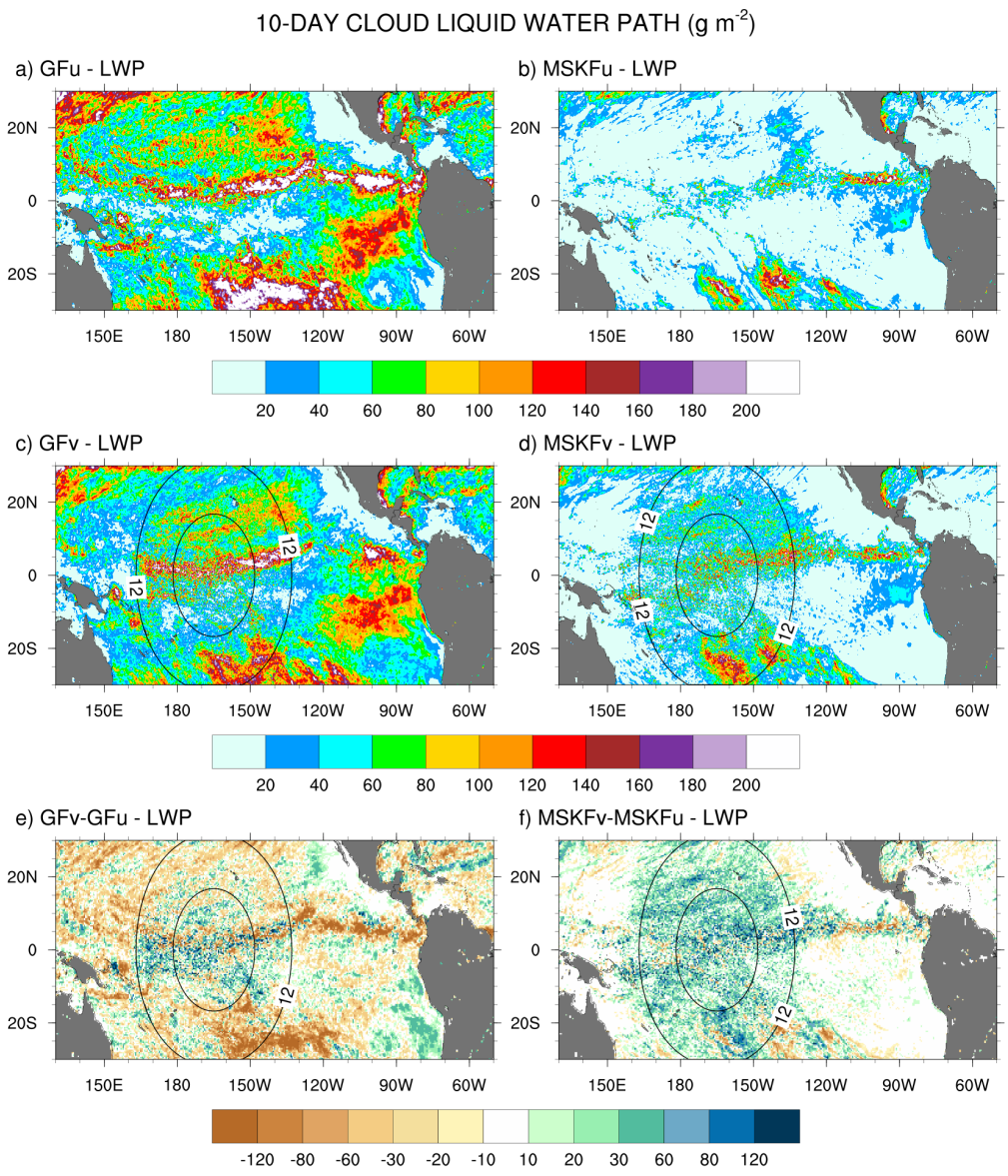

Figure 14r: 10-day mean cloud liquid water path (LWP) over the Tropical Pacific Ocean simulated with GFu and MSKFu (top panels) and GFv and MSKFv (middle panels), and 10-day mean LWP differences between GFv and GFu, and MSKFv and MSKFu (bottom panels).

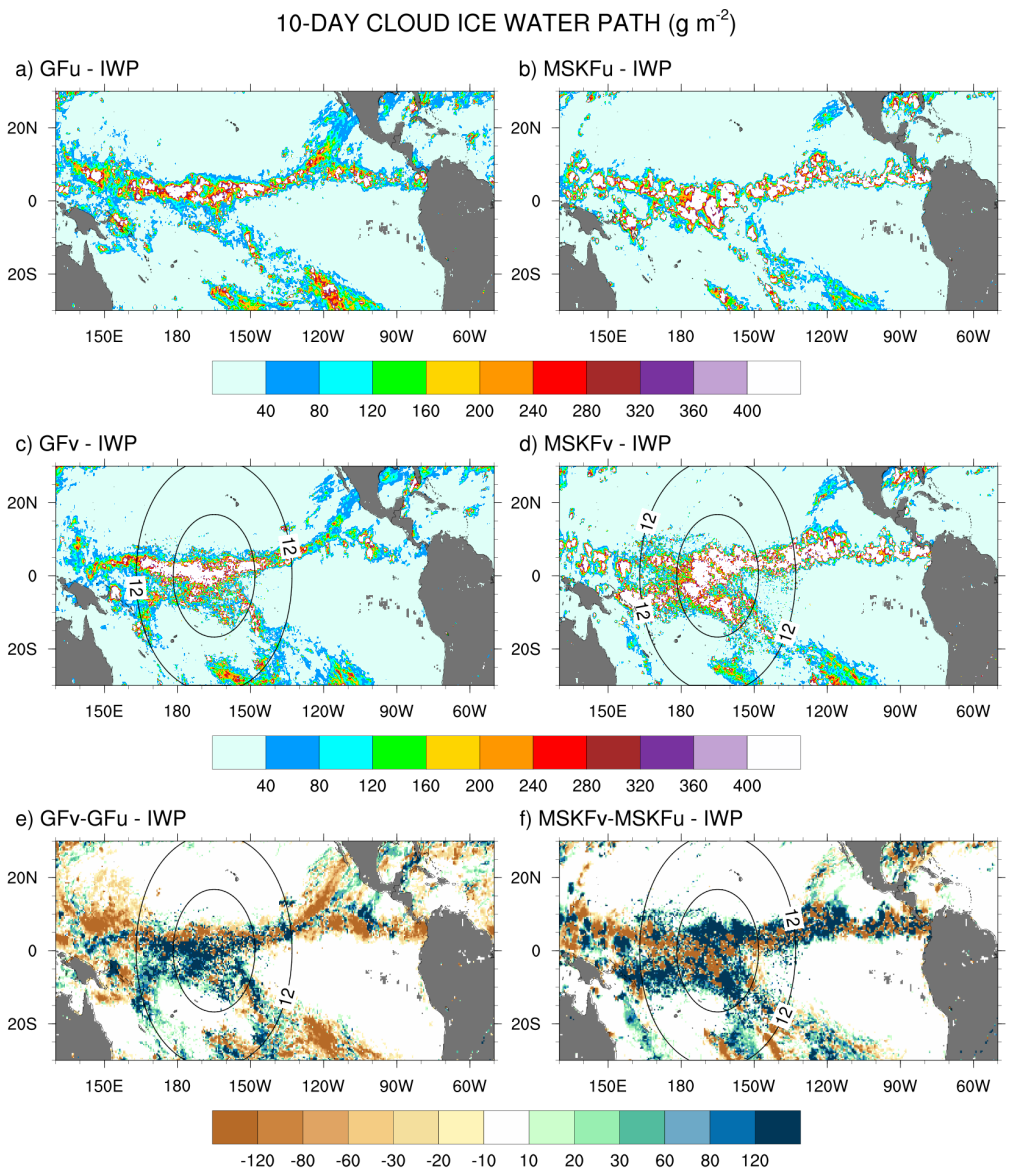

Figure 17r: As Fig. 14r, but for the cloud ice water path (IWP).

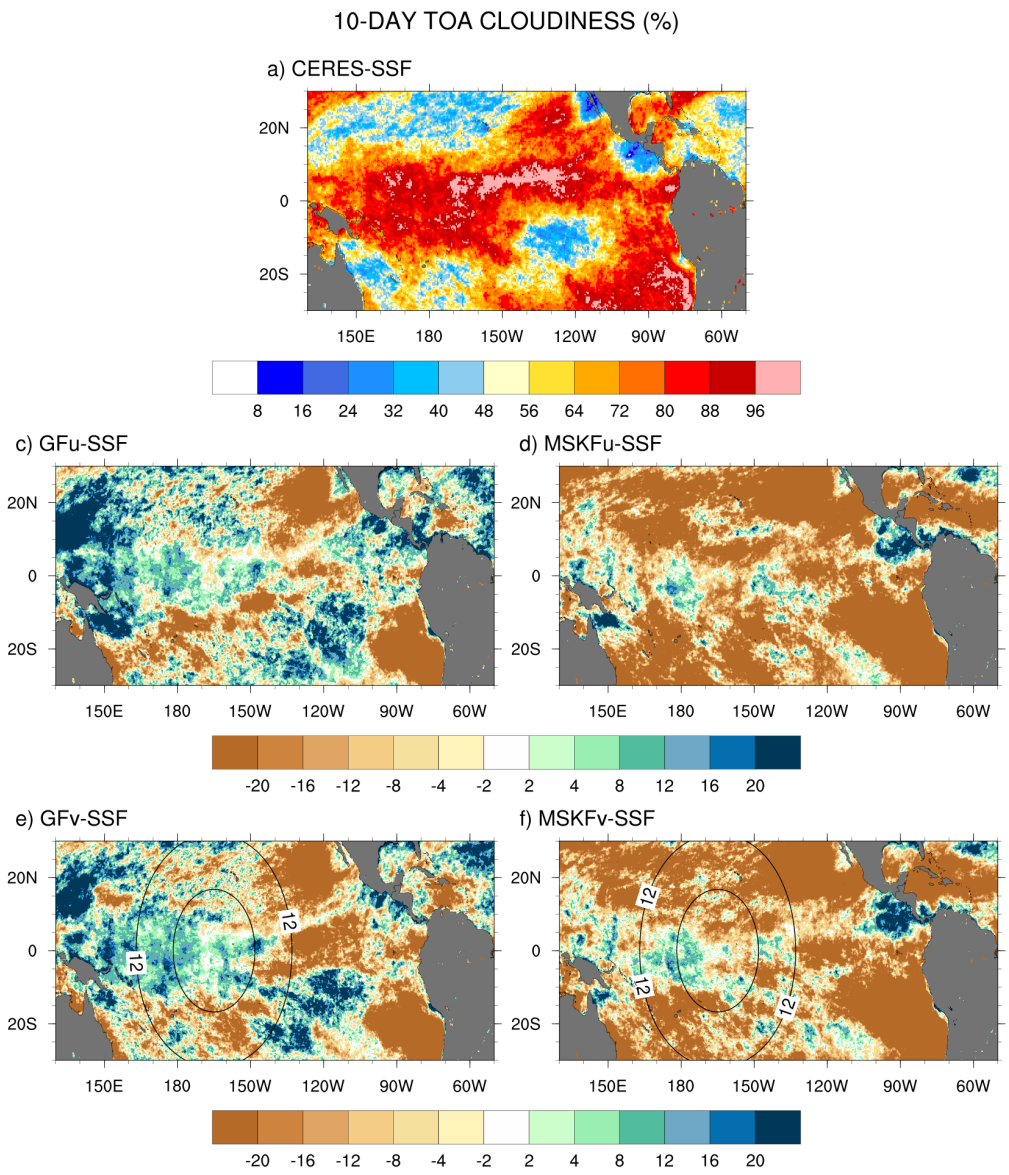

Figure S4r: 10-day mean vertically-integrated cloud fraction (TOACF) over the Tropical Pacific Ocean from a) CERES-SSF data, and difference in the TOACF between GFu (MSKFu) and CERES-SSF (middle panels) and between GFv (MSKFv) and CERES-SSF (bottom panels) for December 2015.

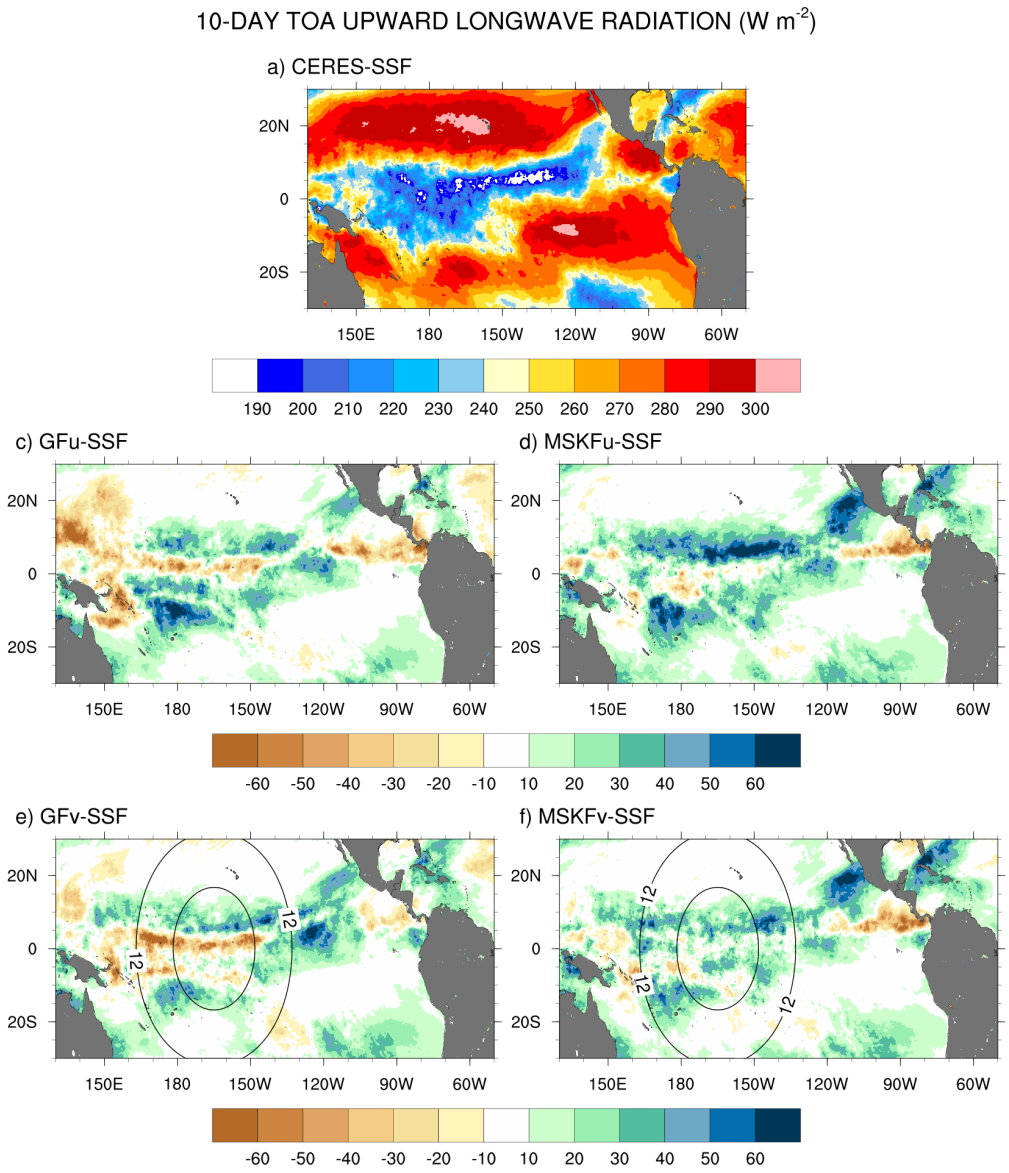

Figure S5r: 10-day mean TOA upward longwave radiation (TOALW) over the Tropical Pacific Ocean from a) CERES-SSF data, and difference in the TOALW between GFu (MSKFu) and CERES-SSF (middle panels) and between GFv (MSKFv) and CERES-SSF (bottom panels).

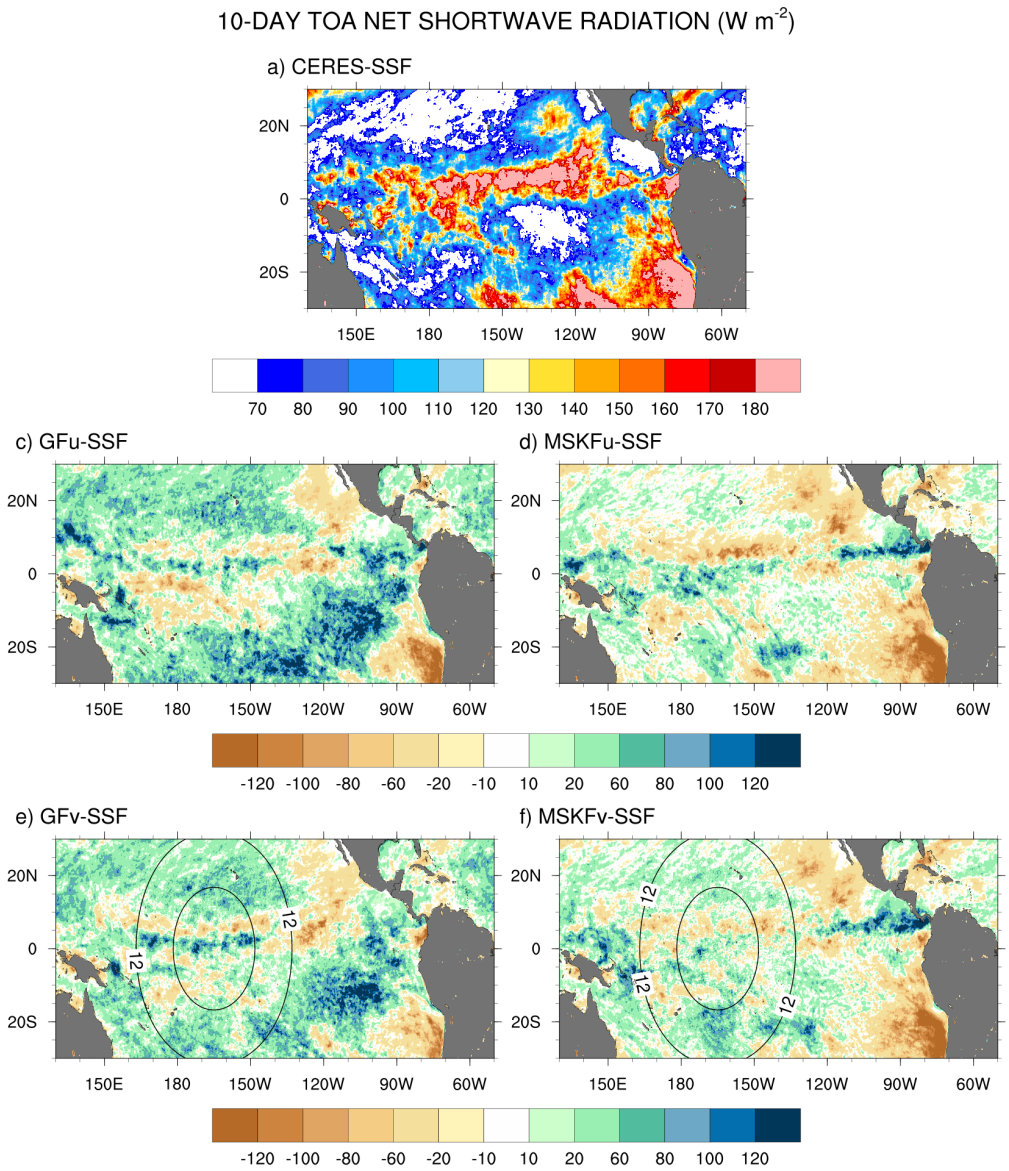

Figure S6r: As Fig. S5r, but for the TOA net shortwave radiation (TOASW).